arXiv:2201.03300v1 [cond-mat.supr-con] 10 Jan 2022

Boron based new high entropy alloy superconductor $Mo_{0.11}W_{0.11}V_{0.11}Re_{0.34}B_{0.33}$

Kapil Motla,[1] Arushi,[1] Pavan K. Meena,[1] and R. P. Singh[1,*]

[1] *Department of Physics, Indian Institute of Science Education and Research Bhopal, Bhopal, 462066, India*

Superconducting high entropy alloys (HEAs) are new members of disordered superconductors. We report the synthesis and investigation of a new superconducting high entropy alloy $Mo_{0.11}W_{0.11}V_{0.11}Re_{0.34}B_{0.33}$ (MWVRB). It crystallized in the tetragonal $CuAl_2$ crystal structure with space group ($I4/mcm$). Comprehensive transport, magnetization and heat capacity measurements confirmed bulk type-II superconductivity having transition temperature $T_C = 4.0$ K. The low temperature electronic specific heat suggests a fully gapped superconducting state in weak coupling limit.

I. INTRODUCTION

High entropy alloys are getting enormous interest in material science due to their unique composition and outstanding properties over conventional alloys [1–3]. The alloy contains at least five constituent elements with 5 to 35 atomic % is called high entropy alloy [4–7], and their inherent feature "high entropy" help to crystallize the random solid solution in simple crystallographic lattice such as in bcc [8], fcc [9], α-Mn [10, 11] and hcp [12] crystal structure [4, 13]. Superconductivity was also observed in some high entropy alloys despite their high disordered nature, where the possibility of regular phonon modes are unlikely [14]. The superconducting phenomenon combined with mechanical properties such as high thermal stability, high strength, and excellent corrosion resistance exhibited in HEAs makes them a promising system for fundamental study as well as for application purposes [15–18]. These high entropy alloy superconductors were reported to show some unconventional properties like retention of superconductivity at extremely high pressure, anomalous broadening in specific heat jump, lattice heat parameter in the elemental range [19, 20] and superconducting parameters similar to phonon mediated superconductors [11]. Understanding the occurrence of superconductivity and exotic properties in these highly disordered and multicomponent alloys remains challenging due to the lack of detailed electronic structure and lattice vibration, which is vital to understanding the superconducting pairing mechanism. The chemical complexity and disorder in the HEAs can provide a versatile platform to investigate the relationship between the property of an ordered to disordered state [21]. Currently, a lot of effort is going on to discover new superconducting high entropy alloys in different crystal structures and tune their superconducting transition temperature using the combination of 3d, 4d, and 5d elements. Same time very few microscopic studies and the unavailability of different families of high entropy alloy superconductors make it difficult to understand the superconducting pairing mechanism [11]. It is clearly important to search for new HEA superconductors to understand the superconducting ground state properties of these emerging new families of disordered superconductor.

In this paper, we report the synthesis and a detailed investigation of the superconductivity in rhenium and boron-rich new HEA superconductor using magnetization, resistivity and heat capacity. It crystallized in a tetragonal $CuAl_2$ crystal structure with space group ($I4/mcm$) and having a superconducting transition temperature 4.0 K. Uemura plot constructed using electronic property calculations places MWVRB in the band of conventional superconductors.

II. EXPERIMENTAL DETAILS

A polycrystalline sample of MWVRB was synthesized using arc melting stoichiometric quantities of Mo(99.95%), W(99.95%), V(99.7%), Re(99.99%), and B(99.5%) in a single arc furnace under high purity argon gas. A Ti getter is used to remove any residual oxygen present in the chamber. The ingot was flipped and remelted several times to ensure sample homogeneity. The resulting sample was shiny, and weight loss was negligible. The phase purity of the sample was confirmed by powder X-ray diffraction on a PANalytical X-Pert Pro diffractometer using Cu-K_α, (λ = 1.5405 Å) radiation at ambient temperature. Macroscopic superconductivity was verified by DC magnetization using a vibrating sample magnetometer (VSM) option of the Quantum Design MPMS 3 (Magnetic Property Measurement System). Transport and heat capacity measurements were carried out using the Quantum Design physical property measurement system (PPMS).

* rpsingh@iiserb.ac.in

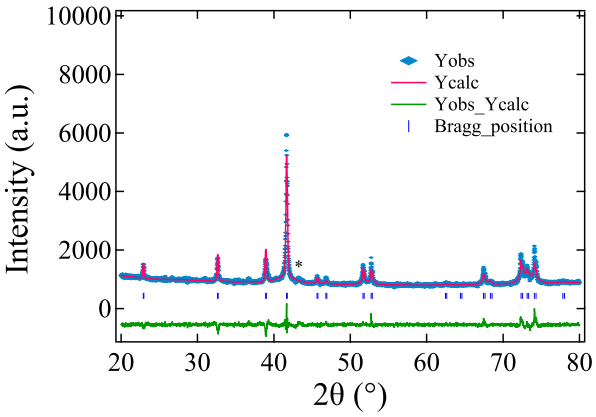


FIG. 1. Powder X-ray diffraction pattern collected at room temperature using CuK_α radiation. The observed pattern is fitted with a tetragonal ($I4/mcm$) structure (solid red line).

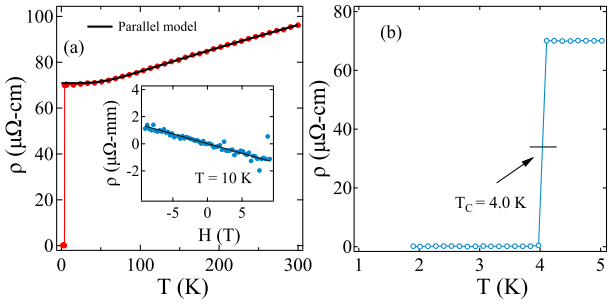


FIG. 2. (a) The temperature dependent resistivity of MWVRB sample in temperature range 1.9 $K \leq T \leq 300$ K is fitted using parallel resistor model by solid black line, and the inset shows the Hall resistivity at 10 K ($> T_C$). (b) The sharp superconducting transition is shown with $T_C = 4.0$ K.

III. RESULTS AND DISCUSSION

a. Structural characterization

The room temperature X-ray diffraction pattern of the as-cast MWVRB sample is shown in Fig. 1. The Le-bail fitting was used to determine the crystal structure and lattice parameters by employing Fullprof software. It confirmed that the MWRVB formed in a tetragonal $CuAl_2$ type crystal structure (space group ($I4/mcm$)) with lattice parameters a = b = 5.4848 Å and c = 4.6240 Å. The broadness of the peak can be attributed to the degree of disorder in this HEA. Despite large atomic difference $Mo_{0.11}W_{0.11}V_{0.11}Re_{0.34}B_{0.33}$ (MWVRB) stabilized in a single phase.

b. Electrical resistivity

Fig. 2(a) shows the temperature-dependent resistivity ρ(T) in the temperature range of 1.9 K to 300 K in zero applied field, and the sharp transition is observed at T_C = 4.0 K [see Fig. 2(b)]. The observed resistivity at room temperature is 71 $\mu\Omega cm$ and the residual resistivity ratio RRR = ρ_{300K}/ρ_{7K} = 1.37 and is comparable with some Re-based binary and HEA superconductors [11, 22, 23]. The low value of RRR may be due to the existence of the atomic-scale disorder and the very small size of the domains in HEAs [8, 24, 25]. $\rho(T)$ above 50 K is found to be linear with temperature and then saturates at high temperatures. Similar trend was also seen in Re_6Zr [26] and BiPd [27] and it is proposed that mean free path in some materials become shorter, which leads to the deviation in resistivity from linearity to saturation [28]. This type of behaviour of $\rho(T)$ was well described using parallel resistor model and expressed as

$$\rho(T) = \left[\frac{1}{\rho_s} + \frac{1}{\rho_i(T)}\right]^{-1} \quad (1)$$

where ρ_s is the saturation resistivity achieved at higher temperatures and $\rho_i(T)$ is ideal temperature dependent resistivity given as

$$\rho_i(T) = \rho_{i,0} + \rho_{i,L}(T) \quad (2)$$

where the first term $\rho_{i,0}$ is temperature-independent residual resistivity. The second term is temperature-dependent, which accounts the phonon-assisted electron scattering and is expressed by the generalized BG resistivity model as

$$\rho_{i,L}(T) = C\left(\frac{T}{\Theta_D}\right)^5 \int_0^{\Theta_D/T} \frac{x^5}{(e^x-1)(1-e^{-x})} dx \quad (3)$$

here C is a material dependent quantity and Θ_D is the Debye temperature, which is obtained from resistivity measurements. The observed resistivity data is well fitted with theoretical red solid line and is shown in Fig. 2(a). The fitting yields ρ_0 = 71.1 $\mu\Omega cm$, $\rho_{0,s}$ = 112 $\mu\Omega cm$, and Θ_D = 335 K, which is in good agreement with the Θ_D obtained from specific heat measurement (discussed later).

c. Magnetization

To ensure bulk superconductivity in the MWVRB sample, DC magnetization measurements were performed in zero field-cooled warming (ZFCW) and field-cooled cooling (FCC) modes in 1 mT magnetic field. The onset of diamagnetism is considered the transition temperature T_C = 4.0(1) K, shown in Fig. 3(a). In the superconducting state, FCC data indicate the strong pinning in MWVRB HEA, and above T_C, sample shows

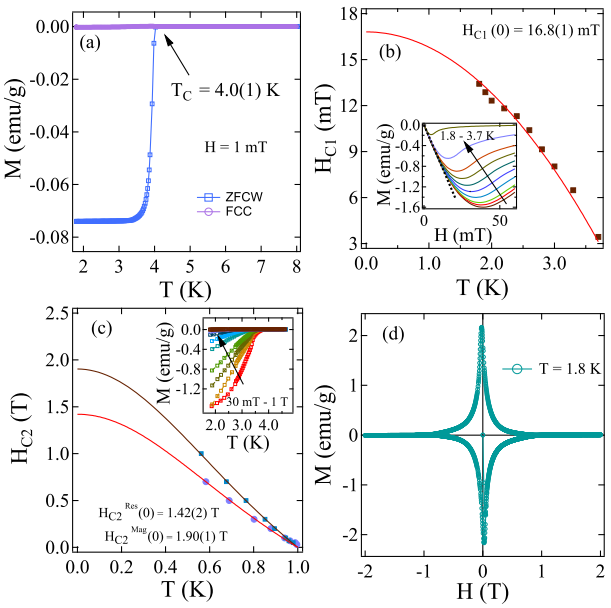


FIG. 3. (a) Temperature dependence of DC magnetic moment in both ZFCW and FCC mode under an applied field of 1 mT. (b) Temperature dependent lower critical field curve fitted with Eq. 4 and inset shows the field dependent magnetization within temperature range 1.8 K to 3.7 K. (c) Temperature dependence of upper critical field fitted with Eq. 5 and inset represents magnetization *vs* temperature within magnetic field range 30 mT to 1 T. (d) The field dependent magnetization M(H) at 1.8 K.

the paramagnetic nature. The temperature and magnetic field dependent magnetization of MWVRB was used to reveal several superconducting state parameters. The lower critical field was evaluated using the field-dependent magnetization (M-H) collected at different temperatures from base value to T$_C$. In the low field range, the field-dependent magnetization data varies linearly and deviates at a particular value of the magnetic field, the so-called lower critical field for that temperature. The evaluated critical field value increases with decreasing temperature, and the observed data is fitted well with the Ginzburg-Landau expression as

$$H_{C1}(T) = H_{C1}(0)\left(1 - \left(\frac{T}{T_C}\right)^2\right) \tag{4}$$

We extrapolate the theoretical curve up to $0K$, which yields the H$_{C1}$(0)= 16.8(1) mT as shown in Fig. 3(b).

Another characteristic parameter, the upper critical field was calculated using the temperature dependent magnetization and resistivity measurements in varying applied magnetic fields [see Fig. 3(c)]. The T_C^{onset} and T_C^{mid} were the criteria of transition temperature for the upper critical field from magnetization and resistivity measurements, respectively. The onset of diamagnetism in magnetization curves shifted towards lower temperature with the application of increasing magnetic fields, as shown in the inset of Fig. 3(c). The $H_{C2}(T)$ *vs* T data were explained very well by the Ginzburg-Landau expression

$$H_{C2}(T) = H_{C2}(0)\left(\frac{1-t^2}{1+t^2}\right) \tag{5}$$

where $t = T/T_C$ is the reduced temperature, and by extrapolate the theoretical curve up to $0K$, we obtained $H_{C2}^{Mag,Res}(0)$ = 1.90(1), 1.42(2) T from magnetization and resistivity measurements, respectively. Furthermore, according to the expression, the upper critical field is directly related to the Gingburg-Landau coherence length as

$$H_{C2}(0) = \frac{\Phi_0}{2\pi\xi_{GL}^2} \tag{6}$$

where Φ_0 is the magnetic quantum flux (Φ_0 = 2.07×10^{-15}T-m^2) and using the value of H$_{C2}$(0) = 1.90(1) T (from magnetization), we obtained the coherence length $\xi_{GL}(0)$ = 13.1(1) nm. The lower critical field is related to the magnetic penetration depth $\lambda_{GL}(0)$ and is defined as

$$H_{C1}(0) = \frac{\Phi_0}{4\pi\lambda_{GL}^2(0)}\left(\ln\frac{\lambda_{GL}(0)}{\xi_{GL}(0)} + 0.12\right) \tag{7}$$

after substituting the values of $\xi_{GL}(0)$ = 13.1(1) nm, and $H_{C1}(0)$ = 16.8(1) mT, it yields the magnetic penetration depth $\lambda_{GL}(0)$ = 160(11) nm, for MWVRB sample.

Ginzburg-Landau provide a parameter κ_{GL}, which can differentiate the types of superconductivity, and expressed in terms of penetration depth $\lambda_{GL}(0)$ and coherence length $\xi_{GL}(0)$ as κ_{GL}=$\frac{\lambda_{GL}(0)}{\xi_{GL}(0)}$, using $\xi_{GL}(0)$ = 13.1(1) nm and $\lambda_{GL}(0)$ = 160(11) nm for MWVRB, we have calculated the κ_{GL} = 12.2(1) » $\frac{1}{\sqrt{2}}$, which indicate that the MWVRB HEA is a type II superconductor. The impact of the applied magnetic field on Cooper pair breaking occurs via two types of mechanism; either the orbital field effect or the Pauli limiting magnetic field effect, which destroys the superconductivity of any material. Using the Werthamar-Helfand-Hohenberg (WHH) model without considering spin-orbit interaction [29], the orbital limiting field in dirty limit BCS superconductor is expressed as

$$H_{C2}^{orbital}(0) = -\alpha T_C \left.\frac{dH_{C2}(T)}{dT}\right|_{T=T_C} \tag{8}$$

where α can take 0.693 value in case of dirty limit superconductivity [discussed later]. Near T$_C$, the variation of temperature dependent upper critical field $\frac{dH_{c2}}{dT}$ is estimated to be -1.2(1) T, which yields the orbital limiting field H_{C2}^{orb} = 3.3(2) T. Another effect which suppresses the superconductivity is Pauli-clogston limiting field H_p and within the BCS theory it can be expressed

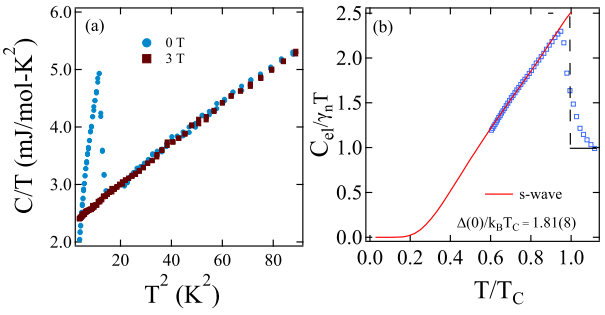


FIG. 4. (a) C/T *vs* T^2 curve at 0 T and 3 T are shown by solid circle and square symbols, respectively. (b) The low temperature specific heat data in the measured temperature range is fitted using the BCS s-wave model.

as $H^P_{c2} = 1.84\ T_C$ [30]. The calculated value of $H^P_{c2} = 7.3(2)\ T$. The estimation of the relative strength of orbital and Pauli limiting field value of the upper critical field is done by determining the Maki's parameter α_M as $\alpha_M = \sqrt{2}H^{orb}_{C2}(0)/H^p_{C2}(0)$. The value of α_M is 0.7 for MWVRB sample, which indicates the significant influence of orbital limiting field over the Pauli paramagnetic field in destroying the superconductivity.

The magnetization hysteresis loop (± 2T) was taken at 1.8 K and shown in Fig. 3(d). At a value of magnetic field (±1T), a closed loop was observed and is called H_{irr}. The value of H_{irr} is below the upper critical field, which is the indication of deppining of vortex flux line in MWVRB HEA.

d. Specific heat

We have performed zero-field specific heat measurement to confirm bulk superconductivity and loss of entropy at T_C in the new superconducting MWVRB HEA. The sharp jump in the specific heat C/T *vs* T^2 data is observed at the bulk superconducting transition temperature $T_C \sim 3.6\ K$ as shown in Fig. 4(a), which coincides with the superconducting transition temperature observed from magnetization and resistivity measurements. Above T_C, the C/T *vs* T^2 data is fitted well with the conventional Debye model as

$$\frac{C}{T} = \gamma_n + \beta_3 T^2 \tag{9}$$

where $\gamma_n T$ and $\beta_3 T^3$ are the electronic and the phononic heat capacity contributions, respectively. The normal state specific heat fitting provides the electronic heat capacity coefficient $\gamma_n = 2.41(4)\ mJ\text{-}mol^{-1}K^{-2}$ (Sommerfeld parameter) and lattice heat capacity coefficient $\beta_3 = 0.027(1)\ mJ\text{-}mol^{-1}K^{-4}$ for MWVRB HEA. The β_3 coefficient is related to Debye temperature as

$$\Theta_D = \left(\frac{12\pi^4 RN}{5\beta_3}\right)^{\frac{1}{3}} \tag{10}$$

where R is the universal gas constant, and N is the number of atoms per unit cell, which is 1. After substituting the related parameters, we calculated the Debye temperature $\Theta_D = 414(7)\ K$. The Debye temperature is higher than conventional alloys and in the range of other high entropy alloy superconductors [10, 11]. The electronic heat capacity constant is proportional to the density of state for the non-interacting system by the expression

$$\gamma_n = \left(\frac{\pi^2 k_B^2}{3}\right) D_C\left(E_F\right) \tag{11}$$

here $k_B = 1.38\times\ 10^{-23} JK^{-1}$ is the Boltzmann constant and the estimated value of density of state at the Fermi level $D_C(E_F)$ is 1.02(2) $\frac{states}{eV f.u}$. The electron-phonon interaction parameter λ_{e-ph}, which gives information regarding the strength between electron and phonon coupling. The λ_{e-ph} is related to Θ_D and T_C, and given by the McMillan model as [31]

$$\lambda_{e-ph} = \frac{1.04 + \mu^* \ln(\theta_D/1.45T_C)}{(1 - 0.62\mu^*)\ln(\theta_D/1.45T_C) - 1.04} \tag{12}$$

where μ^* is the screened Coulomb potential, and the typical value is 0.13 for the intermetallic compound. Using $\Theta_D = 414(7)$ K, $T_C = 3.6\ K$ (from specific heat measurement), the calculated electron-phonon coupling parameter is $\lambda_{e-ph} = 0.54(7)$ that indicates weakly coupled superconductivity in MWVRB system.

In order to estimate the superconducting gap structure and magnitude, the electronic specific heat C_{el} can be estimated by excluding the phononic contribution from the total specific heat $C(T)$ using the expression $C_{el} = C(T)$ - $\beta_3 T^3$. The electronic specific heat data below T_C can be well fitted with isotropic single-gap BCS model for normalized entropy S as

$$\frac{S}{\gamma_n T_C} = -\frac{6}{\pi^2}\left(\frac{\Delta(0)}{k_B T_C}\right)\int_0^\infty [f\ln(f) + (1-f)\ln(1-f)]dy \tag{13}$$

where $f(\xi) = [\exp(E(\xi)/k_BT)+1]^{-1}$ is the Fermi function, $E(\xi) = \sqrt{\xi^2 + \Delta^2(t)}$, where $E(\xi)$ is the energy of the normal electrons relative to the Fermi energy, $y = \xi/\Delta(0)$, $t = T/T_C$ and $\Delta(t) = tanh[1.82(1.018((1/t)$-$1))^{0.51}]$ is the approximation of temperature dependent energy gap by BCS theory. The normalized electronic specific heat in superconducting state is related with the normalized entropy as

$$\frac{C_{el}}{\gamma_n T_C} = t\frac{d(S/\gamma_n T_C)}{dt} \tag{14}$$

The observed electronic heat capacity data below T_C is fitted with Eq. 14 and is shown in Fig. 4(b). The fitting in the measured temperature region provide $\Delta(0)/k_BT_C = 1.81(8)$. The value of gap with λ_{e-ph} indicating the possibility of weakly coupled isotropic superconducting gap in MWVRB HEA.

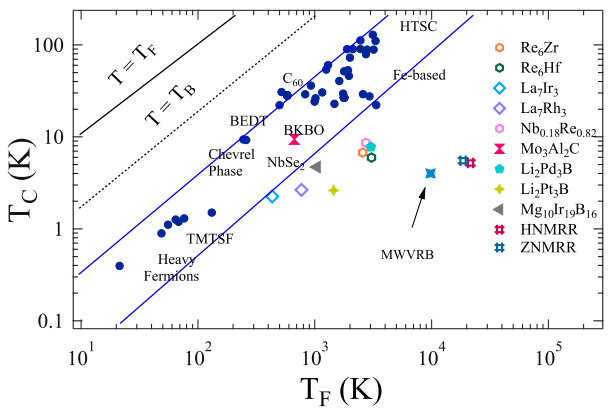


FIG. 5. A plot between the superconducting transition temperature T_C and the Fermi temperature T_F is shown for different superconducting families [11, 32, 33]. The solid blue marker represents the position of MWVRB superconductor which is away from the unconventional band (region between two blue lines).

e. Electronic property and Uemura plot

To obtain the electronic properties such as effective mass, mean free path, and Fermi velocity, we have used some calculated parameters such as charge density n (from hall measurement), Sommerfeld coefficient γ_n (by specific heat measurement), and the residual resistivity ρ_0 (from resistivity measurement). The carrier density n and effective mass of quasi-particles m^* are related to Sommerfeld coefficient γ_n as [34]

$$\gamma_n = \left(\frac{\pi}{3}\right)^{2/3} \frac{k_B^2 m^* n^{1/3}}{\hbar^2} \tag{15}$$

where $k_B = 1.38 \times 10^{-23}\ JK^{-1}$ is Boltzmann constant, after incorporating the parameter values of n, and γ_n, we obtained $m^* = 5.4(1) m_e$. The carrier density n is dependent on effective mass m^* and Fermi velocity v_F by the expression

$$n = \frac{1}{3\pi^2}\left(\frac{m^* v_f}{\hbar}\right)^3 \tag{16}$$

where $\hbar$ is the Planck's constant, and by employing $n = 4.7\times10^{28} m^{-3}$ and $m^* = 5.4(1)\ m_e$, it yields $v_F = 2.35(6) \times 10^5$ ms^{-1}. The mean free path l is related to m^*, ρ_0, and v_F as

$$l = \frac{3\pi^2\hbar^3}{e^2\rho_0 m^{*2} v_F^2} \tag{17}$$

using the previously calculated parameter values, $m^* = 5.4(1)\ m_e$, $v_F = 2.35(6) \times 10^5 ms^{-1}$, and the $\rho_0 = 71\ \mu\Omega$ cm , we get the mean free path $l = 14(1)\ nm$. BCS coherence length ξ_0 can be estimated using the Fermi velocity v_F and the transition temperature T_C via relation

$$\xi_0 = \frac{0.18\hbar v_F}{k_B T_C} \tag{18}$$

using $T_C = 4.0(1)\ K$ (from magnetization) and the evaluated v_F value gives us $\xi_0 = 84(4)\ nm$. We then calculated the ratio of coherence length to the mean free path $\xi(0)/l = 60(7) \gg 1$, which indicates the dirty limit superconductivity in HEA sample. The other evaluated parameter are listed in Table I.

To distinguish MWVRB HEA as conventional or unconventional, we have used Uemura plot classification [32, 35, 36]. If the ratio of T_C/T_F for any superconducting material fall in the region $0.01 \leq T_c/T_F \leq 0.1$, then it is considered as the unconventional superconductor, like the organic, heavy fermions and cuprates superconductors. Superconductors falling in the other region with $T_C/T_F \geq 0.1$ are classified as the conventional superconductors. To estimate the Fermi temperature value, we have used the expression $k_B T_F = \frac{\hbar^2}{2m^*}(3\pi^2 n)^{2/3}$ [37] where k_B is the Boltzmann constant, $m^* = 5.4(1)\ m_e$, and $n = 4.7(2) \times 10^{28} m^{-3}$ which yields $T_F = 9800(357)$ K. The ratio of T_C/T_F is found out to be 0.0004 which places MWVRB HEA far away from the unconventional superconductors [38, 39].

TABLE I. Superconducting and normal state parameters of MoReB[40], WReB [40] and $Mo_{0.11}W_{0.11}V_{0.11}Re_{0.34}B_{0.33}$(MWVRB)

PARAMETERS	UNITS	MoReB	WReB	MWVRB
T_C	K	5.25	5.30	4.0(1)
VEC		5.28	5.28	5.24
$H_{C1}(0)$	mT	13.9	13.3	16.8(1)
$H_{C2}^{mag}(0)$	T	2.1	2.0	1.90(1)
$H_{C2}^{P}(0)$	T	-	-	7.3(2)
ξ_{GL}	nm	12.5	12.8	13.1(1)
λ_{GL}	nm	-	-	160(1)
k_{GL}		15.6	15.7	12.2(1)
$\Delta(0)/k_B T_C$		-	-	1.81(8)
m^*/m_e		-	-	5.4(1)
ξ_0/l_e		-	-	60(7)
v_F	$10^5\ ms^{-1}$	-	-	2.35(6)
n_s	10^{28}m^{-3}	-	-	4.7(2)
m^*/m_e		-	-	5.4(1)
T_F	K	-	-	9800(357)
T_C/T_F		-	-	0.0004

IV. CONCLUSION

In summary, we have synthesized a new superconducting high entropy alloy $Mo_{0.11}W_{0.11}V_{0.11}Re_{0.34}B_{0.33}$ and characterized its normal and superconducting state using magnetization, resistivity, and specific heat measure-

ments. It is crystallized in a $CuAl_2$ type tetragonal crystal lattice with ($I4/mcm$) space group. The magnetization and specific heat capacity measurements confirm the bulk superconductivity at 4.0 K. The electronic heat capacity in the superconducting state is explained well by the conventional BCS model with $\Delta(0)/k_BT_C = 1.81(7)$ superconducting gap value. The other normal and superconducting parameters of MWVRB are listed in Table I along with two ternary alloys, MoReB and WReB (crystallized in similar $CuAl_2$ type structure). Despite the considerable disorder, MWVRB can be classified as a weakly electron-phonon coupled superconductor and share similarity with ternary $CuAl_2$ superconducting family. However, further microscopic measurements such as muon spin rotation/relaxation and theoretical band structure calculations are required to understand the pairing mechanism better. In addition, further superconducting studies on new HEA can help establish a connection regarding the nature of superconducting ground state between ordered and disordered systems.

V. ACKNOWLEDGMENTS

Kapil Motla acknowledges the CSIR funding agency (Award no; 09/1020(0123)/2017-EMR-I), Council of Scientific and Industrial Research (CSIR) Government of India for providing SRF fellowship. R. P. S. acknowledge Science and Engineering Research Board, Government of India for the Core Research Grant CRG/2019/001028.

[1] B. Cantor, I. T. H. Chang, P. Knight, A. J. B. Vincent, Mater. Sci. Eng. A 213, 375 (2004).
[2] E. P. George, D. Raabe, R. O. Ritchie, Nat. Rev. Mater. 4, 515 (2019).
[3] X. Wang, W. Guo, and Y. Fu, J. Mater. Chem. A 9, 663 (2021).
[4] J. W. Yeh, S. K. Chen, S. J. Lin, J. Y. Gan, T. S. Chin, T. T. Shun, C. H. Tsau and S. Y. Chang, Adv. Eng. Mater. 6, 299 (2004).
[5] D. B. Miracle, O. N. Senkov, Acta Materialia 122, 448 (2017).
[6] Y. Zou, J. Mater. Res. 33, 3035 (2018).
[7] J. W. Yeh, S. Y. Chang, Y. D. Hong, S. K. Chen, S. J. Lin, Mater. Chem. Phys. 103, 41 (2007).
[8] P. Koželj, S. Vrtnik, A. Jelen, S. Jazbec, Z. Jagličić, S. Maiti, M. Feuerbacher, W. Steurer and J. Dolinšek, Phys. Rev. Lett. 113, 107001 (2014).
[9] N. Ishizu, J. Kitagawa, arXiv 2020, arXiv:2007.00788.
[10] K. Stolze, F. A. Cevallos, T. Kong and R. J. Cava, J. Mater. Chem. C 6, 10441 (2018).
[11] K. Motla, Arushi, P. K. Meena, D. Singh, P. K. Biswas, A. D. Hillier, R. P. Singh, Phys. Rev. B 104, 094515 (2021).
[12] B. Liu, J. Wu, Y. Cui, Q. Zhu, G. Xiao, S. Wu, G. Cao, and Z. Ren, Scripta Materialia 182 (2020).
[13] M. C. Troparevsky, J. R. Morris, P. R. C. Kent, A. R. Lupini and G. M. Stocks, Phys. Rev. X 5, 011041 (2015).
[14] F. Kormann, Y. Ikeda, B. Grabowski, and M. H. F. Sluiter, npj Computational materials 3, 36 (2017).
[15] Z. Li, K. G. Pradeep, Y. Deng, D. Raabe, and C. C. Tasan, Nature 534, 227 (2016).
[16] S. Rowthu, B. S. Murty, and R. S. Kottade, J. Alloy Compd. 583, 419 (2014).
[17] Y. Zou, S. Maiti, W. Steurer, R. Spolenak, Acta Mater. 65, 85 (2014).
[18] Y. Qiu, S. Thomas, M. A. Gibson, H. L. Fraser, and N. Birbilis, npj Mater. Degrad. 1, 15 (2017).
[19] J. Guo, H. Wang, F.V. Rohr, Z. Wang, S. Cai, Y. Zhou, K. Yang, A. Li, S. Jiang, Q. Wu, R. J. Cava and, L. Sun, PNAS 114, 13144 (2017).
[20] Md. R. Kasem, A. Yamashita, T. Hatano, K. Sakurai, N. O. -Hori, Y. Goto, O. Miura, and Y. Mizuguchi, Supercond. Sci. Technol. 34, 125001 (2021).
[21] F. V. Rohr, M. J. Winiarski, J. Tao, T. Klimczuk, and R. J. Cava, Proc. Natl. Acad. Sci. USA 113, E7144 (2016).
[22] C. S. Lue, H. F. Liu, C. N. Kuo, P. S. Shih, J.-Y. Lin, Y. K. Kuo, M. W. Chu, T.-L. Hung, and Y. Y. Chen, Supercond. Sci. Technol. 26, 055011 (2013).
[23] A. B. Karki, Y. M. Xiong, N. Haldolaarachchige, S. Stadler, I. Vekhter, P. W. Adams, D. P. Young, W. A. Phelan, and J. Y. Chan, Phys. Rev. B 83, 144525 (2011).
[24] S. Marik, M. Varghese, K.P. Sajilesh, D. Singh, R.P. Singh, J. Alloys Compd. 769 (2018).
[25] G. Kim, M. -H. Lee, J. H. Yun, P. Rawat, S. -G. Jung, W. Choi, T. -S. You, S. J. Kim, J. -S. Rhyee, Acta Materialia 186, 250 (2020).
[26] D. A. Mayoh, J. A. T. barker, R. P. Singh, G. Balakrishnan, D. McK. Paul, and M. R. Lees, Phys. Rev. B 96, 064521 (2017).
[27] B. Joshi, A. Thamizhavel, and S. Ramakrishnan, Phys. Rev. B 84, 064518 (2011).
[28] Z. Fisk and G. W. Webb, Phys. Rev. Lett. 36, 1084 (1976).
[29] N. R. Werthamer, E. Helfand, and P. C. Hohemberg, Phys. Rev. 147, 295 (1966).
[30] A. M. Clogston, Phys. Rev. Lett. 9, 266 (1962).
[31] W. L. McMillan, Phys. Rev. 167, 331 (1968).
[32] Y. J. Uemura, L. P. Le, G. M. Luke, B. J. Sternlieb, W. D. Wu, J. H. Brewer, T. M. Riseman, C. L. Seaman, M. B. Maple, M. Ishikawa, D. G. Hinks, J. D. Jorgensen, G. Saito and H. Yamochi, Phys. Rev. Lett. 66, 2665 (1991).
[33] J. A. T. Barker, B. D. Breen, R. Hanson, A. D. Hillier, M. R. Lees, G. Balakrishnan, D. McK. Paul and R. P. Singh, Phys. Rev. B 98, 104506 (2018).
[34] M. Tinkham, Introduction to Superconductivity (McGraw-Hill, New York, 1996).
[35] Y. J. Uemura, V. J. Emery, A. R. Moodenbaugh, M. Suenaga, D. C. Johnston, A. J. Jacobson, J. T. Lewandowski, J. H. Brewer, R. F. Kiefl, S. R. Kreitzman, G. M. Luke, T. Riseman, C. E. Stronach, W. J. Kossler, J. R. Kempton, X. H. Yu, D. Opie and H. E. Schone, Phys. Rev. B 38, 909 (1988).
[36] Y. J. Uemura, G. M. Luke, B. J. Sternlirb, J. H. Brewer, J. F. Carolan, W. N. Hardy, R. Kadono, J. R. Kempton, R. F. Kiefl, S. R. Kreitzman, P. Mulhern, T. M. Riseman, D. L. Williams, B. X. Yang, S. Uchida, H. Takagi, J. Gopalakrishnan, A. W. Sleight, M. A. Subramanian, C. L. Chien, m. Z. Cieplak, G. Xiao, V. Y. Lee, B. W. Statt, C. E. Stronach, W. J. Kossler and X. H. Yu, Phys. Rev. Lett. 62, 2317 (1989).
[37] A. D. Hillier, and R. Cywinski, Appl. Magn. Reson. 13, 95 (1997).

[38] D. A. Mayoh, J. A. T. Barker, R. P. Singh, G. Balakrishnan, D. McK. Paul and M. R. Lees, Phys. Rev. B 96, 064521 (2017).
[39] S. Sundar, S. Salem-Sugui Jr., M. K. Chattopadhyay, S. B. Roy, L. S. Sharath Chandra, L. F. Cohen and L. Ghivelder, Supercond. Sci. Technol. 32, 055003 (2018).
[40] Y. Cui, J. Wu, B. Liu, Q. Zhu, G. Xiao, S. Wu, G. Cao, and Z. Ren, J. Alloy Compd. 832, 154855 (2020).